ELSEVIER

International Journal of Pharmaceutics 242 (2002) 37–46

international journal of pharmaceutics

www.elsevier.com/locate/ijpharm

Structural analysis of nanocapsules by nuclear magnetic resonance

C. Mayer *, D. Hoffmann, M. Wohlgemuth

University of Duisburg, Fakultät 4, Institut für Chemie 47057 Duisburg, Germany

Received 10 December 2001; received in revised form 15 January 2002; accepted 29 January 2002

Dedicated to Prof. Dr. W.S. Veeman on the occassion of his 60th birthday

Abstract

The applicability of nuclear magnetic resonance spectroscopy to dispersed pharmaceutical carriers is demonstrated on poly-*n*-butylcyanoacrylate nanocapsules as a model system. Spectroscopic data are presented that simultaneously reflect the chemical nature and the molecular mobility of individual system components. The results are analysed by numeric simulation procedures that reproduce the spectroscopic results based on the given experimental conditions together with rotational and lateral diffusion of the particles. Under consideration of the complete data set, a comprehensive model on the structure of the nanocapsule system is developed. Details of the model include the assignment of system components to the capsule wall as well as to the internal and the external liquid phase. Further, the capsule size, the permeability of the capsule walls, and molecular adsorption to the capsule surface is observed and determined.

Keywords: Nanocapsules; Structural analysis; Nuclear magnetic resonance; Rotational diffusion; Lateral diffusion; Release

1. Introduction

The characterisation of dispersed nanoparticles as drug carriers often presents a challenging analytical problem. In many cases, physicochemical methods are chosen to determine the physical and chemical structure of these systems and its components. This applies to the particle matrix as well as to other ingredients being either embedded in the particles or dissolved in the surrounding medium. Common spectroscopic techniques such as infrared or UV–vis spectroscopy are very sensitive in the detection of chemical components, however, they generally fail in the determination of structural details. Methods of thermal analysis such as differential scanning calorimetry (DSC) or DTA allow for the identification of phase states and corresponding transitions, but do not provide detailed information on the chemical nature of the individual phases. Electron microscopy often suffers from possible artefacts while optical microscopy is inadequate when applied to sub-micrometer structures.

Some of these gaps may be filled by nuclear magnetic resonance spectroscopy (Westesen and Wehler, 1992, 1993; Westesen et al., 1995). It

* Corresponding author. Tel.: +49-203-307-3317; fax: +49-203-307-3522

E-mail address: hi408ma@uni-duisburg.de (C. Mayer).

0378-5173/02/$ - see front matter
PII: S0378-5173(02)00184-9

combines a completely non-destructive character with the ability to render information on the chemical nature as well as on the molecular or collective mobility of individual components. Any observed chemical constituent may therefore be assigned to a structural part of the dispersion depending on its characteristic motional behaviour. While a liquid or dissolved component in the fluid phase will preserve its full diffusive mobility depending on the overall viscosity, any constituent of the solid structure is more or less immobilised within the solid matrix and will only reflect the motion of the complete particle. Liquid components being enclosed by a solid nanocapsule will undergo limited lateral self-diffusion and hereby can be differentiated from the external fluid phase, which in contrast is characterised by free self-diffusion. In the following, examples are presented which demonstrate the capability of nuclear magnetic resonance spectroscopy to analyse particle structure based on the characteristics of lateral and rotational diffusion of individual system components. The experiments presented here are focused on nanocapsules from poly-n-butylcyanoacrylate as a model system. However, the results are typical and the overall procedure is of general applicability.

2. Materials and methods

2.1. Poly-n-butylcyanoacrylate nanocapsules

The preparation of poly-*n*-butylcyanoacrylate (PBCA) nanocapsules is based on interfacial polymerisation and has originally been proposed in the late seventies (Florence et al., 1979; Couvreur et al., 1979). For this study, the preparation process has been slightly modified by using an acidic organic phase, the procedure is described in detail elsewhere (Wohlgemuth et al., 2000). Basically, an organic phase consisting of 0.25 g of the monomer BCA (Sicomet 6000®, Sichel GmbH, Hannover, Germany), 1.89 g triglyceride oil (Miglyol 812®, Hüls AG, Marl, Germany), and 0.25 ml 0.1 n hydrochloric acid in 25 ml ethanol is gradually injected into an aqueous phase consisting of 1.5 g of a block-copolymer surfactant (Synperonic PE F68®, Fluka GmbH, Buchs, Switzerland) and 95 ml water during vigorous stirring. Hereafter, the resulting suspension is filtered through a sintered glass filter of 9–15 μm pore size.

2.2. Nuclear magnetic resonance measurements

Nuclear magnetic resonance (NMR) experiments have been performed on two different instruments: a Bruker ASX 400 solid state spectrometer with 400 MHz resonance frequency for protons and a Bruker DRX 500 high resolution spectrometer with 500 MHz resonance frequency for protons (source of both instruments: Bruker Analytik GmbH, Karlsruhe, Germany). All experiments were run on the aqueous dispersions of nanocapsules without further sample preparation. Sample sizes vary between 1 ml in a 5 mm glass tube (for the DRX 500) and 4 ml in a 10 mm glass tube (for the ASX 400). Several types of experiments were used.

(a) *^{13}C direct excitation*. In this case, ^{13}C nuclei are excited by a single $\pi/2$ pulse of typically 7 μs duration followed by detection of the ^{13}C signal under full ^{1}H decoupling. Spectra were obtained by Fourier transformation of the free induction decay of the signal. The number of scans varied between 1000 and 10 000 depending on the sample size, the repetition time was 10 s.

(b) *(^{1}H)-^{13}C cross polarisation*. Here, a $\pi/2$ pulse on ^{1}H nuclei is followed by a period of simultaneous irradiation of ^{1}H and ^{13}C nuclei (mixing period with variable duration t_{cp}) where the Hartmann–Hahn condition is fulfilled, that is $\gamma HH1H = \gamma CH^{13}C$ (Hartmann and Hahn, 1962). This yields a strong polarisation of those ^{13}C nuclei that are subject to dipolar coupling with ^{1}H spins. The corresponding free induction decay is detected and Fourier transformed to yield the (^{1}H)-^{13}C cross polarisation spectrum.

(c) *Relaxation of ^{1}H nuclei in the rotating frame*. Basically, two techniques can be used to monitor this relaxation process: In the direct approach, a $\pi/2$ pulse on ^{1}H nuclei is followed by a spin-lock pulse of variable duration t_{SL},

where the lateral ^{1}H magnetisation is locked in a transversal orientation. The intensity of the ^{1}H signal at the end of the spin lock pulse is detected and plotted as a function of t_{SL}. The following free induction decay may be Fourier transformed to yield corresponding spectra. Alternatively, the cross polarisation sequence described before can be extended by a ^{1}H spin lock signal with a duration t_{SL} between the initial $\pi/2$ pulse and the onset of the mixing period. In this case, the intensity of the ^{1}H magnetisation is detected indirectly by the amplitude of the resulting (^{1}H)-^{13}C cross polarisation signal. Both experimental techniques are described in detail elsewhere (Hoffmann and Mayer, 2000). In case of a monoexponential decay of the signal amplitude with t_{SL}, the corresponding time constant is assigned to the spin-lattice relaxation time of ^{1}H nuclei in the rotating frame $T_{1\rho H}$.

(d) *^{1}H Pulsed field gradient echo experiments*. In this case, a stimulated echo sequence on ^{1}H nuclei is combined with the application of two field gradient pulses, the direction of the gradient pointing along the direction of the external magnetic field. An initial $\pi/2$ pulse on ^{1}H nuclei is followed by the first of the gradient pulses. A second $\pi/2$ pulse on ^{1}H nuclei is set at the beginning of a waiting period with a duration as long as 10–200 ms. A final $\pi/2$ pulse is followed by the second field gradient pulse (with Δ being the time delay between the onsets of the two pulsed gradients) and an echo which is analysed for its amplitude and Fourier transformed to yield a line spectrum. In all cases, the duration of the gradient pulses is kept at $\delta = 2$ ms. The decay of the echo intensity with increasing gradient strength G_{max} is a function of the mean square shift of the observed molecules during the waiting period Δ (Kimmich, 1997). More details of the experiment are described elsewhere (Vogt et al., 2000).

2.3. Simulation of NMR experiments

For the analysis of NMR data, the complete experiment is simulated accounting for all experimental conditions and for lateral and rotational diffusion of the particles. System parameters such as the correlation times for lateral and rotational motion are systematically varied until the best fit with the experimental data results. The numeric simulation algorithm is based on a finite grid approximation that includes the particle position and the particle orientation as well as the time axis (Mayer, 1999a,b, 2000, 2001). In case of simpler chemical exchange processes, analytical approximations can be used to predict the outcome of the experiment (Hoffmann and Mayer, 2000).

3. Results

3.1. Direct excitation

The most straightforward approach in nuclear magnetic resonance is direct excitation of the observed nuclei, which is especially sensitive to liquid and dissolved components. Fig. 1 (top) shows the result of a ^{13}C direct excitation experiment on a dispersion of poly-*n*-butylcyanoacrylate nanocapsules. Reference spectra of single constituents of the dispersion (Fig. 1, bottom) allow for an assignment of the resonance lines. While all signals of the triglyceride and the surfactant are present in the spectrum of the dispersion, no traces of the monomer can be detected (see arrows in Fig. 1, top). Compared with the reference spectra, all line widths have increased for the components of the dispersion (e.g. from 0.29 to 0.42 ppm for the methyl peak of the triglyceride and from 0.27 to 0.32 ppm for the methylene peak of the surfactant). A complete assignment of all peaks is given elsewhere (Hoffmann and Mayer, 2000).

3.2. Cross polarisation

The technique of (^{1}H)-^{13}C cross polarisation relies on a transfer of magnetisation from ^{1}H to ^{13}C nuclei that works most efficiently in case of solid state components. Fig. 2 shows the result for a dispersion of poly-*n*-butylcyanoacrylate nanocapsules together with a reference spectrum

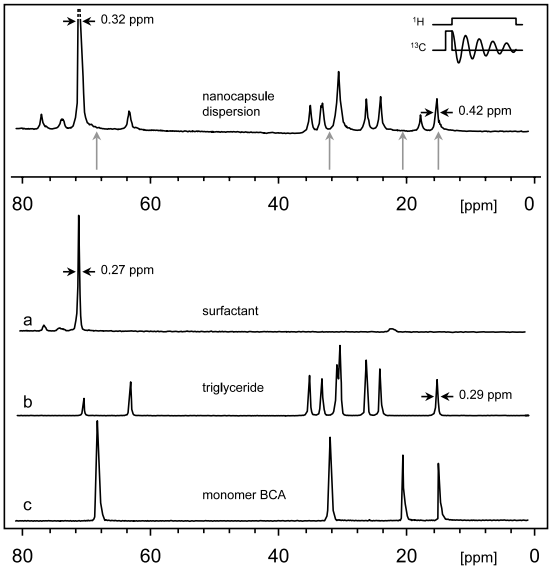

Fig. 1. Top: Direct-excitation ^{13}C spectrum of an aqueous suspension of poly-*n*-butylcyanoacrylate nanocapsules under full proton decoupling. Only the section between 0 and 80 ppm is displayed. Below, corresponding direct-excitation ^{13}C spectra of reference samples. (a) An aqueous solution of the surfactant Synperonic F68® (0.5 g/100 ml), (b) a sample of the pure liquid triglyceride (Miglyol 812), (c) a sample of the liquid monomer *n*-butylcyanoacrylate.

taken on a compact solid sample of the polymer PBCA. The characteristic wide lines of five carbon resonances occurring in the spectral region between 0 and 100 ppm are reproduced in the spectrum of the dispersion. Despite a relatively poor signal to noise ratio in the latter, it can be stated that the line widths are basically identical. In addition to the broad solid state lines, the cross polarisation spectrum of the dispersion also shows narrow lines that correspond to the resonances of the triglyceride and the surfactant (compare Fig. 1).

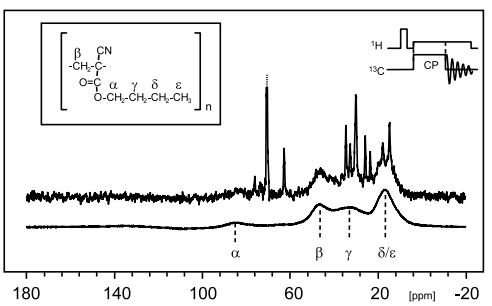

Fig. 2. Comparison between a (^1H)-^{13}C cross polarisation spectrum of dispersed nanocapsules from poly-n-butylcyanoacrylate (top) with the corresponding spectrum of a solid reference sample of the compact polymer (below). In both cases, a mixing period of duration $t_{cp} = 0.5$ ms is used. The insert (top, right) is a graphic representation of the applied pulse sequence.

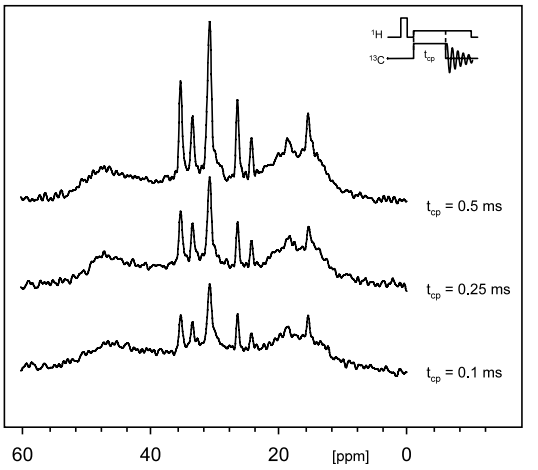

Fig. 3. (^1H)-^{13}C cross polarisation spectra of dispersed poly-*n*-butylcyanoacrylate nanocapsules ($\omega_C/2\pi \cong 100$ MHz, full proton decoupling) for three different contact times ($t_{cp} = 0.1$, 0.25 and 0.5 ms). At $t_{cp} = 0.25$ ms, the broad signals of the polymer have almost reached their full intensity, whereas the signals of the components in the liquid phase still gain amplitude. The insert (top, right) is a graphic representation of the applied pulse sequence.

The wide and narrow lines in the cross polarisation spectrum of the dispersion significantly differ in their dependence on the mixing time t_{cp} (Fig. 3). While the broad lines of the solid contributions are almost fully developed at $t_{cp} = 0.1$ ms, the narrow lines of the components in the fluid phase (triglyceride and surfactant) need more than 0.5 ms to reach their peak amplitude.

3.3. Spin-lattice relaxation in the rotating frame

All organic constituents of the nanocapsule dispersion have been studied for the spin-lattice relaxation in the rotating frame of ^1H nuclei. Interesting results are obtained for the triglyceride

and the surfactant, typical relaxation curves are shown in Fig. 4. Direct excitation measurements (Fig. 4, right column) yield the expected monoexponential decays with relaxation times ranging from 34 ms for the α-methylene group of the triglyceride to 131 ms for the dominating methylene group of the surfactant. On the other hand, determinations of the ^{1}H relaxation curves via cross polarisation of the corresponding carbon segments lead to strongly biexponential plots (Fig. 4, left column). Interestingly, the two relaxation times that describe the initial and the final part of the slope correspond to those of the solid polymer component and to those obtained in direct excitation, respectively (Hoffmann and Mayer, 2000).

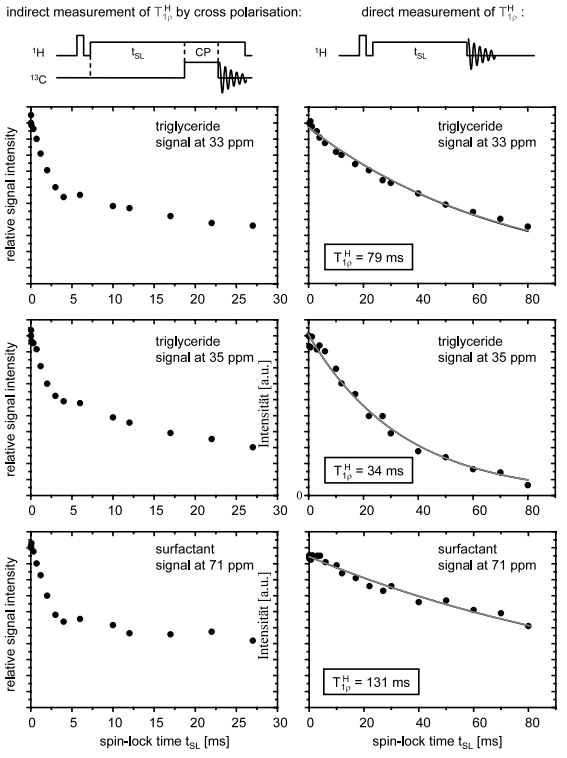

Fig. 4. Pulse sequences and relaxation curves for determination of spin-lattice relaxation times in the rotating frame of hydrogen nuclei in an aqueous poly-*n*-butylcyanoacrylate nanocapsule dispersion, (a) as detected indirectly by the intensity of carbon signals in a cross polarisation experiment (left column), (b) as detected directly by the intensity of the corresponding hydrogen signals (right column).

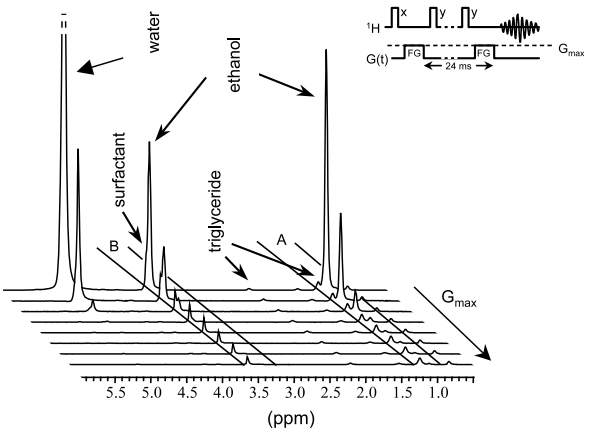

Fig. 5. Fourier transformed proton echo signals from a stimulated echo PFG experiment on dispersed poly-*n*-butylcyanoacrylate nanocapsules ($\omega_H/2\pi \cong 500$ MHz, $\Delta = 24$ ms) with increasing pulse gradient strength G_{max}. The strongest signals can be assigned to water (4.8 ppm) and ethanol (3.6 and 1.15 ppm, multiplets not resolved). The peaks characterising the ingredients of the capsule system (surfactant at 3.65 ppm as well as triglyceride at 1.2 and 2.2 ppm) are hardly visible at weak gradients, but dominate the spectrum at stronger gradients.

3.4. Pulsed field gradient echo experiments

For reasons of sensitivity, the pulsed field gradient (PFG) experiments are limited to ^{1}H nuclei of liquid phase components of the nanocapsule system. Fig. 5 shows a stacked plot of spectra that derive from Fourier transformed PFG echo signals at a common gradient pulse spacing of $\Delta = 24$ ms and increasing gradient strengths G_{max}. Under these conditions, the echo decay reflects the lateral mobility of the individual system constituents within a time frame of 24 ms. While the resonances of water (at 4.8 ppm) and of residual ethanol (at 3.6 and 1.15 ppm) decrease very rapidly with increasing G_{max}, the signals for the surfactant (at 3.65 ppm) and the triglyceride (at 1.2 and 2.2 ppm) seem to be affected to a much smaller extent.

As the peaks for the surfactant and the triglyceride overlap with the ethanol resonances, the quantitative analysis of the decay curves is performed on the signal groups 'A' and 'B' (Fig. 5) rather than on the individual resonances. Figs. 6 and 7 show the dependence of their relative echo intensity E_{rel} on the spacing Δ between the gradi-

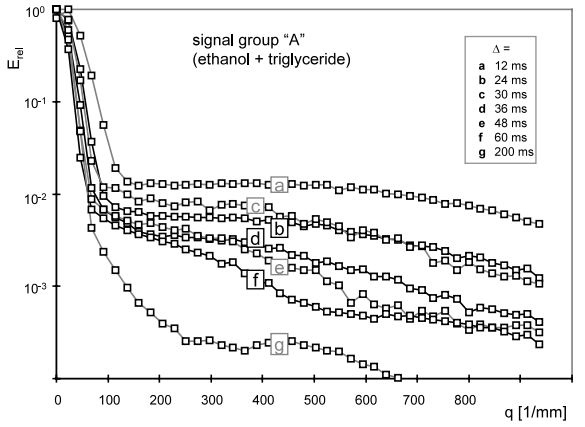

Fig. 6. Relative echo intensities of the signal group 'A' (ethanol and triglyceride, see Fig. 5) depending on the wave vector $q = \gamma\delta G_{max}/2\pi$ and on the pulse separation Δ. The duration of the gradient pulses is kept constant at 2 ms, the pulse separation varies between 12 and 200 ms.

ent pulses and on the wave vector q. The latter is determined by the gradient strength G_{max} according to $q = \gamma\delta G_{max}/2\pi$, where γ stands for the gyromagnetic ratio of ^{1}H nuclei and $\delta = 2$ ms for the duration of the gradient pulses. While the decay curves of the signal group A clearly show two separate components (Fig. 6), the decay curves for the signal group B consist of three subunits characterised by different slopes (Fig. 7). Even if the final plateau for signal group B is generally low in intensity and severely affected by the absolute experimental error, the values for $\Delta > 30$ ms are distinctly above the noise level and therefore indicate a significant signal contribution which remains even for $q > 500$ mm^{-1} (Fig. 7).

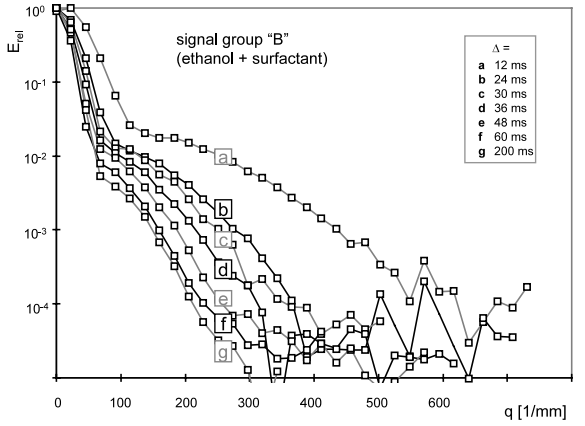

Fig. 7. Relative echo intensities of the signal group 'B' (ethanol and surfactant, see Fig. 5) depending on the wave vector $q = \gamma\delta G_{max}/2\pi$ and on the pulse separation Δ. The duration of the gradient pulses is kept constant at 2 ms, the pulse separation varies between 12 and 200 ms.

4. Discussion

4.1. Assignment of system components

The most obvious difference between carbon line spectra of solid components and those of constituents of the liquid phases is the line width of the ^{13}C signals, which generally is much larger in the first case. A second indicator for molecules in the solid phase is their tendency to generate enhanced signals under cross polarisation conditions. Therefore, the wide lines in the cross polarisation spectrum in Fig. 2 (top) can be positively assigned to the solid structure of the capsules. Its similarity to the reference spectrum of PBCA (Fig. 2, bottom) indicates that the vast majority of the solid structure is formed by this polymer. In contrast to other cases (Mayer and Lukowski, 2000; Mayer, 2001), it was not necessary to run NMR sample spinning experiments for a detailed analysis of the solid under the given conditions.

All organic molecules in the liquid phases undergo rapid rotational diffusion and therefore lead to high resolution ^{13}C resonances that are easily assigned to the various reference spectra (Fig. 1). According to a comparison between the direct excitation spectrum and the reference signals, the triglyceride as well as the surfactant occurs in the liquid phases. All liquid phases at the same time lack any traces of monomer or polymer (arrows in Fig. 1, top).

Rotational diffusion serves as a sufficient criterion to differentiate between the solid and the liquid phase state. However, for assignment to the liquid phases inside and outside the capsule walls, lateral diffusion has to be taken into account. In the pulsed field gradient experiment, the signals of the triglyceride at 1.2 and 2.2 ppm show a very shallow decay with increasing gradient strength (Fig. 5). This is reflected by the small slope of the

final sections of the decay curves in Fig. 6, which correspond to a self diffusion constant of 2×10^{-12} m^2 s^{-1} (Wohlgemuth, 2001). This is about an order of magnitude smaller than the self diffusion constant of pure oil (2.3×10^{-11} m^2 s^{-1}), but equivalent to the Brownian motion of spherical particles with a hydrodynamic radius of 120 nm in water at room temperature. Therefore, it can be concluded that the triglyceride forms the inside of the nanocapsules, and that its long range dislocation for large Δ is dominated by the Brownian motion of the capsules.

The decay characteristics of the surfactant in the nanocapsule system (peak at 3.65 ppm in Fig. 5) do not differ significantly from those of the surfactant in aqueous solution. In both cases, a self diffusion constant of 4.5×10^{-11} m^2 s^{-1} is observed, which in water at room temperature corresponds to particles with approximately 10 nm in diameter. This is in good accordance with the expected size of surfactant micelles (Zhou and Chu, 1988). Therefore, it can be assumed that the majority of the surfactant occurs in micelles in the continuous aqueous phase outside of the nanocapsules.

The water, finally, behaves exactly as expected for free water in an aqueous environment, no hindered diffusion is detected for its single proton resonance near 4.8 ppm (Fig. 5). Seemingly, the water molecules are completely restricted to the outside of the nanocapsules. However, this does not completely rule out the possibility of a small water content inside the capsules that undergoes rapid exchange with the outside phase.

4.2. Determination of capsule size

The radius a of a spherical particle in a fluid medium determines the correlation time τ of its rotational diffusion and the self diffusion coefficient D corresponding to its Brownian motion according to

$$\tau = \frac{4\pi\eta a^3}{3kT} \quad \text{and} \quad D = \frac{kT}{6\pi\eta a}$$

where η, k and T stand for the viscosity of the fluid medium, the Boltzmann constant and the temperature, respectively. Based on NMR data, there are three possible approaches for the determination of the capsule size (Mayer, 2001): (a) characterisation of rotational diffusion of the particles by an analysis of the NMR line shape, (b) determination of the Brownian motion of the particles from the PFG decay curves of encapsulated components for long pulse separations, and (c) determination of the hindered self diffusion inside the particles from the PFG decay curves of encapsulated components for short pulse separations.

Unlike other cases (Mayer and Lukowski, 2001; Mayer, 2001), the line shape analysis of the solid state spectrum using numerical simulation procedures (Fig. 2, top) does not yield reliable data on the given system. This is partially due to the poor quality of the spectrum. Moreover, the difference between the reference line shape and the corresponding solid state spectrum of the dispersion seems negligible. Under these conditions, it may only be stated that the particle radius is larger than 100 nm, otherwise significant narrowing of the signals would be observed. This even holds after partial thermal degradation of the capsule walls (data not shown).

However, the PFG data allow for reliable size determination combining the approaches b and c. The decay curves for signal group 'A' (see Figs. 5 and 6) were fitted using a numerical simulation procedure under variation of the capsule size as a single parameter. The best fit, obtained for a mean capsule radius of 120 nm, is shown in Fig. 8 for $\Delta = 24$, 36 and 48 ms. As the shape of the decay curves is very sensitive to the capsule size, the result seems to be quite reliable. The experimental error of this fit is expected to be smaller than 20%. The resulting particle radius is in good accordance with the result obtained by optical observation of the Brownian motion, which yields a number average of 132 nm (Wohlgemuth, 2001).

4.3. Adsorption to the capsule wall surface

The presence of signals from the triglyceride and the surfactant in the cross polarisation spectrum (Fig. 2, top) indicates that these components come into close contact with the solid capsule walls. However, the polarisation transfer from ^{1}H

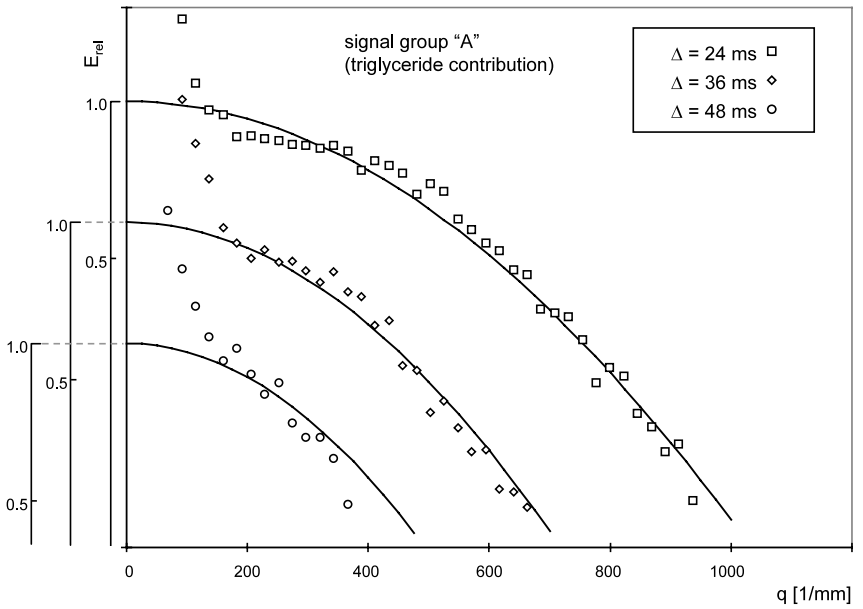

Fig. 8. Contribution of the triglyceride to the echo decay curve of the signal group 'A' for three different pulse separations ($\Delta = 24$ ms, 36 ms, and 48 ms). Smooth lines represent the calculated best fit under variation of the capsule radius as single variable parameter which is obtained for $a = 120$ nm. The scale for the relative echo amplitude E_{rel} is shifted to reduce overlap between the plots for better visibility.

to ^{13}C nuclei is strongly delayed for these components as compared with the solid polymer (Fig. 3). The relaxation behaviour of the cross polarisation signals (Fig. 4, left column) is biexponential and consists of an steep initial slope which corresponds to the solid capsule wall and a final tailing which resembles the relaxation of the fluid phase measured by direct excitation (Fig. 4, right column). Based on these experimental data, a mechanism of cross polarisation is proposed which includes a temporary adsorption of the triglyceride and the surfactant molecules to the capsule walls (Hoffmann and Mayer, 2000). This cross polarisation mechanism allows for the analysis of the adsorption time scale for both components. A simulation of the ^{1}H spin-lattice relaxation in the rotating frame based on this assumption (Fig. 9) yields average durations for the adsorption periods of triglyceride and the surfactant of 3 and 1 ms, respectively (Hoffmann and Mayer, 2000). These numbers are in accordance with results for non-ionic surfactants by a different NMR technique, which led to values between 13.4 and 7 ms for diluted dispersions with a tendency to shorter adsorption periods at higher concentrations (Schönhoff and Södermann, 1997).

4.4. Determination of capsule permeability

An interesting observation is made for the ethanol signals in the ^{1}H pulsed field gradient experiment (Figs. 5–7). The ethanol clearly dominates the initial decay (Figs. 6 and 7) but also contributes, observable for signal group 'B', to the final plateau in the decay curves (Fig. 7). From the slopes of both contributions, it is clear that the steep part of each decay curve corresponds to the 'free' fraction of the ethanol, while the plateau represents the encapsulated fraction. Interestingly, the level of the plateau (E_{rel} for $q > 500$ mm^{-1}) seems to depend on the gradient pulse spacing, with a big step between $\Delta = 12$ and 24 ms (Fig. 7). The amount of ethanol that remains encapsulated during the complete experiment obviously decreases with increasing length of the observation

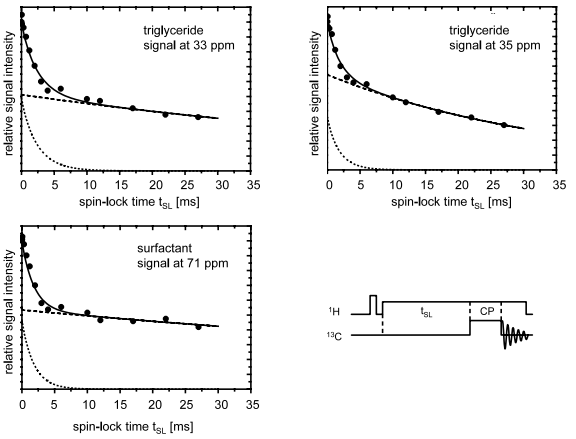

Fig. 9. Comparison between simulated and experimental relaxation curves on liquid components in a dispersion of poly-*n*-butylcyanoacrylate nanocapsules obtained under variation of the spin-lock duration t_{SL}. Full lines represent simulations assuming adsorption periods of 3 ms for the triglyceride (peaks at 33 and 35 ppm) and 1 ms for the surfactant (peak at 71 ppm). Broken lines mark the contributions of permanently liquid or dissolved components, while dotted lines stand for the contributions of molecules being subject to temporary adsorption.

period. That is, the capsules 'leak' ethanol, which of course is not lost but instead takes part in a steady state exchange process with 'free' ethanol through the capsule membrane (Mayer, 2001). A numeric simulation of the decay curves (Figs. 10 and 11) yields an approximate average rate constant of 120 s^{-1} for the exchange process. This corresponds to a half life time for encapsulated ethanol of approximately 6 ms. After this period, half of the ethanol originally encapsulated at $t = 0$ is replaced by molecules from the continuous phase. This finding may serve as a valuable information on the permeability of the capsule walls and the release properties of the capsule system. Similar experiments are extended to active ingredients and suitable model compounds. For long term release studies, they may be performed in a time resolved manner under a wide variety of external conditions.

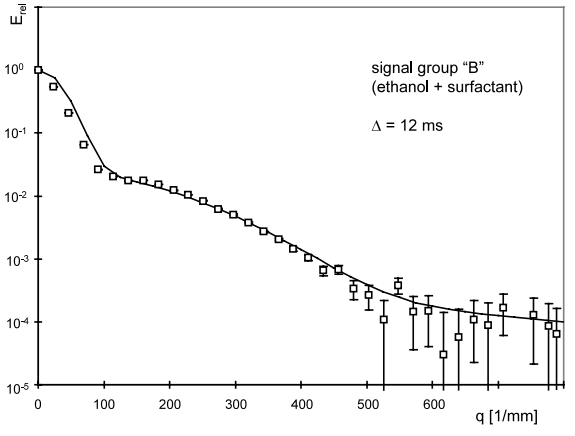

Fig. 10. Best result of a one parameter fit to the PFG echo decay at $\Delta = 12$ ms obtained for an exchange rate of $\bar{k}_{ex} = 120$ s^{-1} (black line). Error bars denote the experimental uncertainty of the individual data.

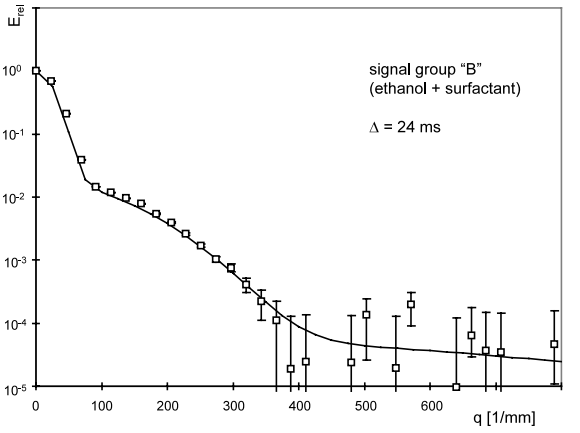

Fig. 11. Best result of a one parameter fit to the PFG echo decay at $\Delta = 24$ ms obtained for an exchange rate of $\bar{k}_{ex} = 120$ s^{-1} (black line). Error bars denote the experimental uncertainty of the individual data.

4.5. Conclusion and outlook

Nuclear magnetic resonance experiments together with corresponding numeric simulation procedures yield a comprehensive model on the structure of nanoparticles that is demonstrated on the example of poly-*n*-butylcyanoacrylate nanocapsules. With little additional information (e.g. the spherical shape of the capsules), a set of detailed information is obtained which is summarised in Fig. 12. It contains data on static structure as well as on dynamic processes. Further techniques, extending the applicability of the NMR approach, are under development.

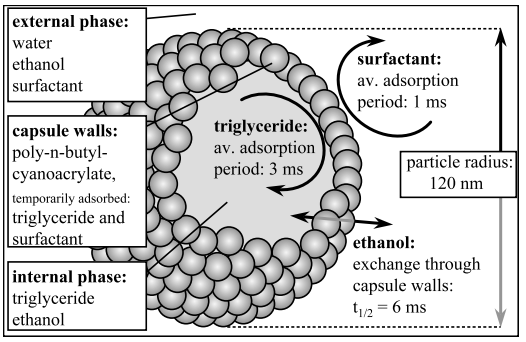

Fig. 12. Graphic representation summarising the structural data obtained from NMR measurements on poly-*n*-butylcyanoacrylate nanocapsules.

5. Uncited reference

Westesen and Wehler, 1992.

References

Couvreur, P., Kante, B., Roland, M., Guiot, P., Baudhuin, P., Speiser, P., 1979. Polycyanoacrylate nanocapsules as potential lysosomotropic carriers: preparation, morphological, and sorptive properties. J. Pharm. Pharmacol. 31, 331–332.

Florence, A.T., Whateley, T.L., Wood, D.A., 1979. Potentially biodegradable microcapsules with poly (alkyl 2-cyanoacrylate) membranes. J. Pharm. Pharmacol. 31, 422–424.

Hartmann, S.R., Hahn, E.L., 1962. Nuclear double resonance in the rotating frame. Phys. Rev. 133, 1108–1122.

Hoffmann, D., Mayer, C., 2000. Cross polarisation induced by temporary adsorption: NMR-investigations on nanocapsule dispersions. J. Chem. Phys. 112, 4242–4250.

Kimmich, R., 1997. NMR, Tomography, Diffusometry, Relaxometry. Springer, Berlin.

Mayer, C., 1999a. Lineshape calculations on spreadsheet software. J. Magn. Reson. 138, 1–11.

Mayer, C., 1999b. Calculation of MAS spectra influenced by slow molecular tumbling. J. Magn. Reson. 139, 132–138.

Mayer, C., 2000. Calculation of cross-polarisation spectra influenced by slow molecular tumbling. J. Magn. Reson. 145, 216–229.

Mayer, C., 2001. Kernmagnetische Resonanz an nanopartikulären Systemen. Deutscher Wissenschafts-Verlag, Würzburg.

Mayer, C., Lukowski, G., 2000. Solid state NMR investigations on nanosized carrier systems. Pharm. Res. 17, 486–489.

Schönhoff, M., Södermann, O., 1997. PFG-NMR diffusion as a method to investigate the equilibrium adsorption dynamics of surfactants at the solid/liquid interface. J. Phys. Chem. B 101, 8237–8242.

Vogt, M., Flemming, H.-C., Veeman, W.S., 2000. Diffusion in *Pseudomonas aeruginosa* biofilms: a pulsed field gradient NMR study. J. Biotechnol. 77, 137–146.

Westesen, K., Wehler, T., 1992. Physicochemical characterization of a model intravenous oil-in-water emulsion. J. Pharm. Sci. 81, 777–786.

Westesen, K., Wehler, T., 1993. Investigation of the particle size distribution of a model intravenous emulsion. J. Pharm. Sci. 82, 1237–1244.

Westesen, K., Gerke, A., Koch, M.H.J., 1995. Characterization of native and drug-loaded human low density lipoproteins. J. Pharm. Sci. 84, 139–147.

Wohlgemuth, M., 2001. Diffusionsexperimente an Nanokapselsuspensionen. Ph.D. thesis, University of Duisburg, Germany.

Wohlgemuth, M., Mächtle, W., Mayer, C., 2000. Improved preparation and physical studies of polybutylcyanoacrylate nanocapsules. J. Microencaps. 17, 437–448.

Zhou, Z., Chu, B., 1988. Light-scattering study on the association behaviour of triblock polymers of ethylene oxide and propylene oxide in aqueous solution. J. Colloid Interf. Sci. 126, 171–180.